第32卷第12期 焊 接 学 报 Vol. 32 No. 12
2011年12月 TRANSACTIONS OF THE CHINA WELDING INSTITUTION December 2011

镀锌钢–6016铝合金异种金属加入中间夹层铅的激光焊接

彭 利，周惦武，吴 平，张 屹*
（湖南大学 汽车车身先进设计制造国家重点实验室，长沙 410082）

摘 要： 对1.2 mm厚镀锌钢板和1.15 mm厚6016铝合金平板试件进行了加入中间夹层铅的激光搭接焊试验，通过调整焊接工艺参数获得最佳焊接成形，利用卧式金相显微镜、扫描电镜、X射线衍射、微机控制电子万能试验机等手段研究了焊接接头各区域的金相组织、断口形貌、主要物相与接头力学性能. 结果表明，在钢/铝激光焊中添加中间夹层铅，焊接接头的平均抗拉强度和断后伸长率分别为68.51 MPa和2.37%，与没有加铅夹层相比，抗拉强度和断后伸长率明显提高；夹层铅的加入，改变了钢/铝界面的元素分布、物相组成及微观组织形态，焊接接头过渡区域Fe，Al，Zn，Mg，Pb元素的混合区宽度较大，除生成Fe–Al，Mg–Zn脆性金属间化合物外，产生了新的金属间化合物Mg_2Pb，改善了焊缝金属的力学性能.

关键词： 激光焊接；异种金属；金属间化合物；微观组织
中图分类号： TG113.26+3 **文献标识码：** A **文章编号：** 0253–360X(2011)12–0081–04

彭 利

0 序 言

汽车车身多材料结构要求两种不同类型的材料进行连接（如钢/铝、铸铁/铝、铝/镁等），对钢/铝异种金属材料连接而言，两者之间的固溶度很低，物理、化学性能差异明显，极易反应生成FeAl脆性金属间化合物[1,2]. 由于传统熔焊的热输入量大，热源难以准确控制，而激光焊接热量集中，应力应变小，因此激光焊是钢/铝的理想的焊接方法[3-5]，FeAl脆性金属间化合物也成为影响激光焊接接头性能的主要因素.

通过以汽车车身用镀锌钢与6016铝合金为研究对象，进行激光搭接焊试验，以中间夹层的方式加入Pb元素钎料，期望通过铅的加入，使钢/铝之间实现良好熔合. 此外改变钢/铝界面的元素分布、物相组成及微观组织形态，铅替换FeAl脆性金属间化合物中元素，或形成较高金属性、延性与塑性的新金属间化合物，以改善钢/铝焊接接头的力学性能. 激光焊接钢/铝的探索研究可为激光焊接多材料车身结构提供重要的理论指导和技术支持.

1 试验方法

试验采用DC025型板条式CO_2激光器及五轴联动激光加工设备，激光器最大输出功率2 500 W，连续输出的激光模式为TEM00，输出能量近似高斯分布. 光束发散半角$\alpha < 0.15 \times 10^{-3}$ rad，抛物面反射聚焦镜焦距为200 mm，焦斑直径为0.4 mm.

试验材料为100 mm × 30 mm × 1.2 mm的DC56D+ZF镀锌钢和100 mm × 30 mm × 1.15 mm的6016铝合金的板材，材料的主要化学成分如表1，表2所示.

表1 DC56D+ZF镀锌钢的化学成分（质量分数，%）
Table 1 Chemical compositions of DC56D+ZF zinc-coated steel sheet

C	Si	Mn	P	S	Fe
0.014	0.008	0.118	0.014	0.030	余量

表2 6016铝合金的化学成分（质量分数，%）
Table 2 Chemical compositions of 6016 aluminum alloy

Si	Mg	Fe	Zn	Mn	Cu	Al
1.0~1.5	0.25~0.6	<0.5	<0.2	<0.2	<0.2	余量

收稿日期：2010–12–05
基金项目：国家863高技术研究发展计划资助项目（2007AA042006）；国家自然科学基金资助项目（50805045）；湖南大学汽车车身先进设计制造国家重点实验室自主课题资助项目（71075003）
* 参加此项研究工作的还有陈根余

将镀锌钢板与 6016 铝合金组合后用夹具夹紧进行激光搭接焊试验，激光束垂直入射到上板表面，随着光束的移动在搭接部位形成连续的激光焊缝. 焊接过程中，采用氩气经拉伐尔喷嘴对熔池区进行保护. 为提高焊缝质量，焊接前用丙酮对铝板和镀锌钢板的待焊表面进行清洗，以去除油污.

考虑到激光焊时铝反射率高，钢比铝更能有效地吸收激光，试验时将聚焦激光作用在镀锌钢板一侧，但是，得到的焊缝结果并不理想，焊缝上表面凹陷，存在较多夹杂和气孔等缺陷. 同时钢铝焊接过程中，两者极易反应生成脆性金属间化合物，严重恶化了钢铝焊接接头的力学性能. 为此利用激光深熔焊原理，提出以中间夹层的方式加入 Pb 元素钎料，接头形式如图 1. 聚焦激光束作用在镀锌钢板/中间夹层/6016 铝合金板三层板上，在获得平整、连续、夹杂缺陷少的焊缝及优质焊接接头的基础上，通过试验得到表 3 的优化工艺参数.

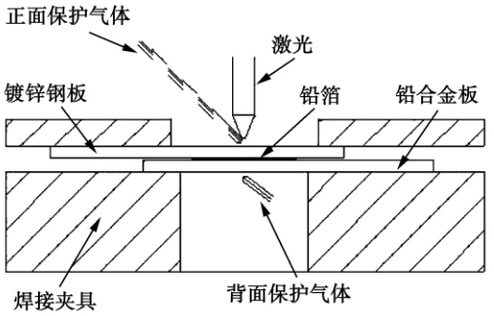

图 1 钢/铝搭接焊原理示意图

Fig. 1 Setup of steel/Al laser lap welding

表 3 钢/铅/铝焊接工艺优化参数

Table 3 Optimized welding parameters

激光功率 P/W	焊接速度 v/(m·min^{-1})	焦点位置 D/mm	保护气体流量 q/(L·min^{-1})
1 600	1 100	−0.5 ~ +1	Ar 20

焊后，利用体视显微镜观察钢/铝焊缝的表面形貌，分析焊缝的成形性与表面质量；线切割取样、打磨抛光试样及质量分数为 4% 的 HNO_3 溶液腐蚀后制备金相试件，利用卧式金相显微镜分析钢/铝焊缝/母材的金相组织；采用 FEI Quanta200 电子扫描电镜自带能谱 EDS 检测分析焊缝的元素混合区的宽度；采用西门子 D500X 射线能谱仪分析焊缝区的主要物相；利用微机控制电子万能试验机分析焊接试件的抗拉强度与断后伸长率；采用电子扫描电镜分析焊接试件的断口形貌，分析试件的断裂机制.

2 试验结果及讨论

2.1 焊缝的表面成形性

焊缝成形性是激光焊接性能的重要影响因素. 对焊缝成形性进行研究有利于改善激光焊接工艺，提高焊缝的可靠性及焊接质量. 图 2 为钢/铅/铝焊缝宏观形貌. 图 2a 为加铅夹层后焊缝上表面的外观，焊缝形貌平整连续，成形均匀一致，无明显的气孔、裂纹等缺陷存在，接头变形小. 图 2b 为此焊缝的横截面形貌，发现除存在少数气孔缺陷外，钢/铝金属间熔合较好，与未加铅夹层相比，熔池的深宽比明显加大，熔池的深宽比大约为 2∶1. 由激光能量转变而来的热能使夹在中间的铅箔迅速熔化，液态铅在铝表面得到铺展并润湿. 热能的快速增加，必然发生 Fe，Al，Pb 等元素的扩散与迁移. 所以这种加入中间夹层铅的扩散连接有利于实现钢/铝异种金属材料之间良好熔合.

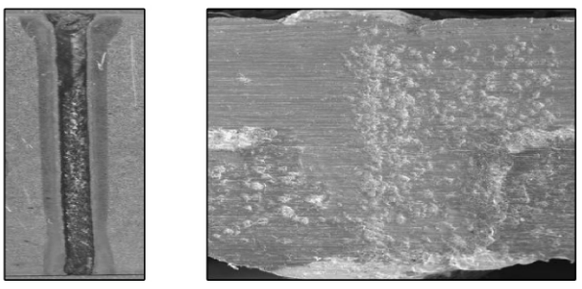

(a) 焊缝上表面 (b) 焊缝横截面

图 2 钢/铅/铝焊缝宏观形貌

Fig. 2 Macro-morphologies of steel/Pb/Al weld

2.2 焊接接头的显微组织

图 3 为钢/铅/铝焊接接头显微组织. 对钢/铝焊缝界面处的结合情况，采用高倍金相显微镜对焊缝钢侧的界面局部放大，见图 3a，发现在钢侧母材与焊缝界面区由母材侧较大晶粒和焊缝的细小晶粒交错形成，没有明显的分界线，为正常的的激光深熔焊特征. 图 3b 为整个熔池形貌，下层铝合金未受浸蚀作用，熔池中存在富铝的白色溶质. 焊缝接头部分，可以看出熔池金属与母材铝之间的良好结合. 靠铝侧边界存在白色粗大的针状相. 从 Al-Pb 偏晶合金的平衡凝固过程来看，在凝固过程中两液相存在较大的密度差异，富铅的 L2 相会聚集下沉并向铝板扩散，出现比重偏析，这种组织的出现对改善焊缝的性能，对强度、硬度等极为有利.

2.3 焊接接头的力学性能

在进行力学性能测试时，试样的尺寸为 90 mm

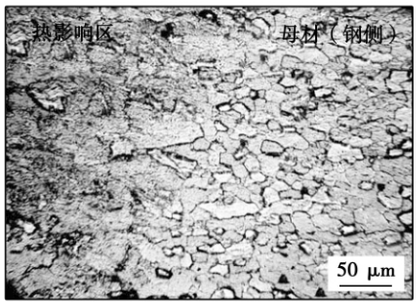

(a) 钢侧的热影响区和母材区

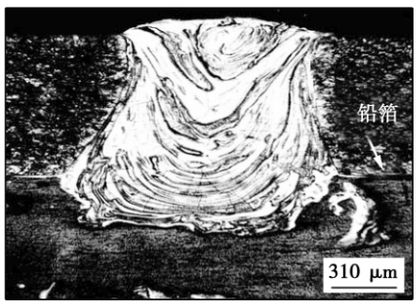

(b) 熔池形貌

图 3　钢/铅/铝焊接接头的显微组织

Fig. 3　Microstructure of steel/Pb/Al joint

×20 mm,焊缝位于中心位置,宽为 10 mm. 图 4 为拉伸试样的断裂位置,可以看到图 4a 的断裂位置为焊缝中心,而图 4b 的拉伸试样断裂在母材(靠铝侧)位置. 图 5 为加夹层前后焊接接头的平均抗拉强度与断后伸长率. 发现添加铅夹层后,平均抗拉强度为 68.51 MPa,比没有添加铅夹层的接头平均抗拉强度提高 75% 左右,而同样情况下,断后伸长率提高 142%.

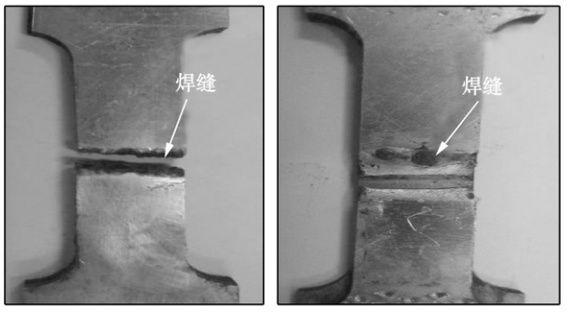

图 4　拉伸试样的断裂位置

Fig. 4　Fracture location of tensile specimen

图 6 为加入夹层前后试样断口形貌. 分析发现,图 6a 断口呈脆性特征,微观形貌为准解理断裂,并带有疲劳条纹特征. 图 6b 断面上呈现了大量的抛物线形韧窝和撕裂特征,整个断面为韧窝断裂.

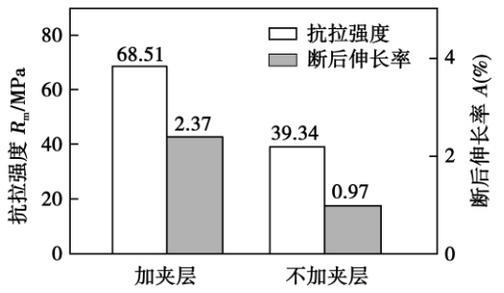

图 5　钢/铝焊接接头抗拉强度与断后伸长率

Fig. 5　Tensile strength and elongtion of steel/Al joint

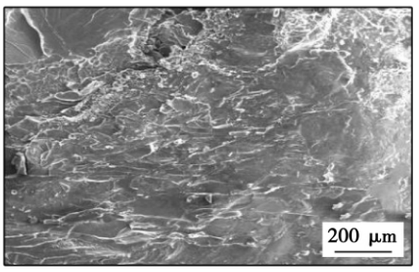

(a) 钢/铝试样断口形貌

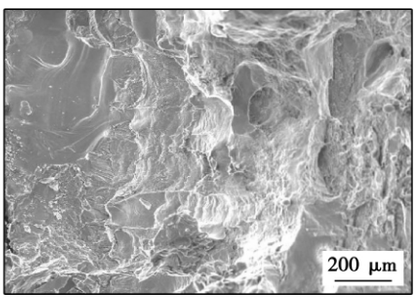

(b) 钢/铅/铝试样断口形貌

图 6　拉伸试样断口形貌

Fig. 6　Morphology of fractured tensile testing sample

2.4　焊接接头的能谱和 XRD 分析

图 7 为焊接接头焊缝横向 EDS 元素的相对含量测试结果. 从图 7 可看出,Fe,Al,Zn,Mg,Pb 元素的混合区宽度较大,与焊缝宽度相当,元素 Fe 和 Al 充分混合且较均匀,这极易促使 FeAl 脆性金属间化合物的生成. 由于激光焊接时加热集中,中心温度高,金属层快速熔合、凝固,导致原子扩散驱动力很大,使得不同区域的各元素相互扩散,如 Pb 元素,从图 7 可看出,钢/铝焊接试样靠铝侧铅含量较高,因此 6016 铝合金基体中的主要成分 Mg 元素与中间夹层中的 Pb 元素可能发生反应形成 Mg-Pb 化合物; 此外镀锌钢板中较高含量的锌,由于 Fe,Al,Zn,Mg,Pb 元素充分混合,也很可能与 Mg 元素发生反应形成 Mg-Zn 化合物.

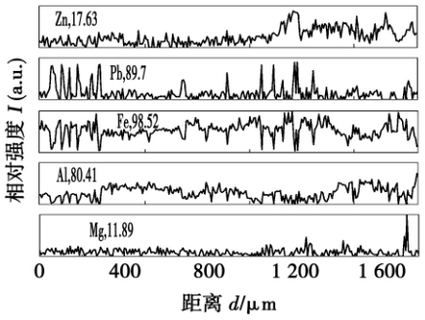

图 7 钢/铅/铝焊接接头焊缝线扫描位置及结果

Fig. 7 Position and results of element line scanning

图 8 为加铅夹层后钢/铅/铝焊接接头 X 射线衍射结果. 分析发现，除生成 $Al_{0.4}Fe_{0.6}$，Mg_2Zn_{11} 等金属间化合物外，焊缝界面还形成了 Mg_2Pb 金属间化合物. 焊接接头物相检测证实了 EDS 分析生成 Mg-Pb，Mg-Zn 等化合物的推测结果. 由于加入中间夹层铅后，除生成 Fe-Al，Mg-Zn 脆性金属间化合物[4]外，产生了新的金属间化合物 Mg_2Pb，由于 Mg_2Pb 延性较好[6,7]，因此有利于改善焊缝金属的力学性能.

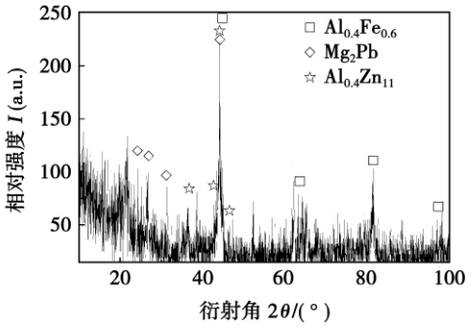

图 8 钢/铅/铝焊接接头相结构的 X 射线衍射图

Fig. 8 X-ray diffraction patterns of phase structure

3 结 论

(1) 镀锌钢与 6016 铝合金激光搭接焊，加入中间夹层铅，焊接接头的平均抗拉强度和断后伸长率分别为 68.51 MPa 和 2.37%，与未加夹层铅相比，抗拉强度和断后伸长率明显提高.

(2) 添加中间夹层铅，镀锌钢与 6016 铝合金焊接接头界面之间熔合良好，界面元素分布、物相组成及微观组织形态发生改变，除生成 Fe-Al，Mg-Zn 脆性金属间化合物外，还形成了新的 Mg_2Pb 金属间化合物，由于 Mg_2Pb 金属间化合物延性较好，因此有利于改善焊缝金属的力学性能.

(3) 镀锌钢与 6016 铝合金激光搭接焊，加入中间夹层铅，钢侧母材与焊缝界面区由母材侧较大晶粒和焊缝的细小晶粒交错形成，没有明显的分界线，为正常的激光深熔焊.

参考文献:

[1] 李亚江. 特种连接技术 [M]. 北京: 机械工业出版社, 2007.

[2] 刘中青，刘 凯. 异种金属焊接技术指南 [M]. 北京: 机械工业出版社, 1997.

[3] 雷 振，王旭友，王伟波，等. 铝/镀锌钢复合热源熔-钎接头中的 Al-Fe 金属间化合物层分析 [J]. 焊接学报, 2007, 28(11): 65-71.
Lei Zhen, Wang Xuyou, Wang Weibo, *et al*. Analysis for Al-Fe intermetallic compomds layer of fusionbrazed joints between aluminium and zinc-coated steel by hybrid welding [J]. Transactions of the China Welding Institution, 2007, 28(11): 65-71.

[4] 倪加明，李俐群，陈彦宾，等. 铝/钛异种合金激光熔钎焊接头特性 [J]. 中国有色金属学报, 2007, 17(4): 617-626.
Ni Jiaming, Li Liqun, Chen Yanbin, *et al*. Characteristics of laser welding-brazing joint of Al/Ti dissimilar alloys [J]. The Chinese Journal of nonferrous metals, 2007, 17(4): 617-626.

[5] Torkamany M J, Tahamtan S, Sabbaghzadeh J. Dissimilar welding of carbon steel to 5754 aluminum alloy by Nd: YAG pulsed laser [J]. Materials Design, 2010, 31(1): 458-465.

[6] Rodrigues D M, Loureiro A, Leitao C. Influence of friction stir welding parameters on the microstructural and mechanical properties of AA 6016-T4 thin welds [J]. Materials Design, 2009, 30(6): 1913-1921.

[7] Duan Y H, Sun Y, Feng J, *et al*. Thermal stability and elastic properties of intermetallics Mg_2Pb [J]. Physica B, 2010, 405(2): 701-704.

作者简介: 彭 利，女，1986 年出生，硕士研究生. 主要从事汽车轻量化材料的激光焊接及数值模. Email: 2009123pengli@163.com

通讯作者: 周惦武，男，博士，教授. Email: zdwe_mail@yahoo.com.cn

well as the coarsen rate of Cu_6Sn_5 particles in the Sn matrix during aging process was both restrained by Nd addition, which would enhance the reliability of the solder joint during service process. Moreover, during aging process, the shear strength reduction rate of SAC-0.05Nd solder joint was lower than that of SAC, but the shear strength reduction rate of SAC-0.5Nd solder joint showed no obvious difference compared with that of SAC because of the coarsen of $NdSn_3$ phase in aging process.

Key words: rare earth Nd; Sn3.8Ag0.7Cu solder; microstructure; shear strength

Microstructure of Mo-Cu alloy and 18-8 stainless steel joint by TIG with filler metal WANG Juan, LI Yajiang, ZHENG Deshuang, JIANG Qinglei (Key Laboratory for Liquid-Solid Structural Evolution & Processing of Materials, Ministry of Education, Shandong University, Jinan 250061, China). p 77 - 80

Abstract: The joining of Mo-Cu alloy with 18-8 stainless steel was carried out by tungsten inert-gas arc welding with filler wire. Microstructure, microhardness, element distribution and phase constituents near the fusion zone of Mo-Cu alloy/18-8 stainless steel joint were investigated by using optical microscopy, scanning electron microscop, microhardners and X-ray diffraction method. Results showed that there were mixed phases of martensite and austenite in the fusion zone at side of Mo-Cu alloy and austenite-ferrite dual phase in the weld metal and fusion zone near 18-8 stainless steel. The formation of carbonized layer in the fusion zone was promoted by the diffusion of Mo from Mo-Cu alloy to weld metal. The phase constituents near the fusion zone at side of Mo-Cu alloy were Mo, Cu, γ-Fe (Ni), $Fe_{0.54}Mo_{0.73}$ and $Cu_{3.8}Ni$. The existence of carbonized layer and $Fe_{0.54}Mo_{0.73}$ intermetallic compound resulted in a higher microhardness of 1 200 HV.

Key words: Mo-Cu alloy; 18-8 stainless steel; tungsten inert-gas arc welding with filler metal; microstructure

Laser lap welding of zinc-coated steel and 6016 aluminum alloy with Pb interlayer PENG Li, ZHOU Dianwu, WU Ping, ZHANG Yi, CHEN Genyu (State Key Laboratory of Advanced Design and Manufacturing for Vehicle Body, Hunan University, Changsha 410082, China). p 81 - 84

Abstract: The laser lap welding experiment with the Pb interlayer was carried out based on the DC56D + ZF galvanized steel of 1.2 mm and the 6016 aluminum alloy of 1.15 mm. The best appearance of welding were obtained by adjusting the welding parameters. By using optical microscopy, scanning electron microscopy, X-ray diffraction and the tensile test, mechanical properties of joints, fracture morphology and the main phase of the welded joint regional was studied. The results showed that when Pb interlayer was added in steel/aluminum, the average tensile strength and elongation of the steel/aluminum laser welding joints were 68.51 MPa and 2.37% respectively. Compared with that without Pb interlayer, the strength and alongation were improved significantly. The element distribution, phase composition and microstructure of the steel/aluminum interface were changed by the addtion of Pb interlayer. In the transition region of steel/aluminum joints, Fe, Al, Zn, Mg, Pb elements of the mixing zone width was larger, and a new ductile intermetallic compounds-Mg_2Pb was produced, which could improve the mechanical properties of weld metal.

Key words: laser welding; dissimilar metal; intermetallic compounds; microstructure

Effects of different solders on mechanical properties of micro-joints soldered with diode-laser soldering system LAI Zhongmin[1], ZHANG Liang[2], WANG Jianxin[1] (1. School of Materials Science & Engineering, Jiangsu University of Science and Technology, Zhenjiang 212003, China; 2. School of Mechanical & Electrical Engineering, Xuzhou Normal University, Xuzhou 221116, China). p 85 - 88

Abstract: Wettability of SnAgCu/SnAgCuCe solders on Cu substrate and properties of solder joints were tested by diode laser soldering system. The solder joints reliability during thermal cycling test was investigated by diode laser soldering system and IR reflow soldering method respectively. The results indicate that, as the laser output power increases, the spreading area of lead-free solder increases, the optimal wettability and spreadability are obtained while the laser output power increases to a certain range. Moreover, the results indicate that the wettability and spreadability of the two kinds of solders on Cu substrate are improved with the increase of heating time under the condition of selected laser output power. For QFP256 devices soldered with diode laser soldering system, optimum power can be found, the optimum power for SnAgCu solders is 16.7 W, for SnAgCuCe solders, it is 17 W. Moreover, during thermal cycling, the reliability of soldered joints obtained by diode laser soldering is higher than that by IR reflow soldering.

Key words: diode laser soldering system; wettability; laser output power; reliability

Fracture toughness of friction stir welded Invar 36 alloy at low temperature ZHAO Yue[1], WU Aiping[1], YUTAKA S. Sato[2], HIROYUKI Kokawa[2] (1. Key Laboratory for Advanced Materials Processing Technology, Ministry of Education, Department of Mechanical Engineering, Tsinghua University, Beijing 100084, China; 2. Department of Materials Processing, Graduate School of Engineering, Tohoku University, 6-6-02 Aramaki-aza-Aoba, Sendai 980-8579, Japan). p 89 - 92

Abstract: The fracture toughness of friction stir welded Invar36 alloy, obtained with travelling speed of 2 mm/s and rotational speed from 200 r/min to 1 000 r/min, were estimated at low temperature (77 K) by small punch test, and were compared with that at room temperature (298 K) as well. At 298 K, all welds have higher small punch energy than the base material. For the welds acquired with the same welding parameters, the small punch energy tested at 77 K is always higher than the ones at 298 K. The small punch energy of welds trends to increase with decreasing of the rotational speed at both 77 K and 298 K. With rotational speeds equal or less than 400 r/min, the small punch energy of welds is significantly higher than that of the base material at 77 K. The results indicate that the friction stir welds keep excellent ductility at low temperature. With the increase of travelling speed, higher heat input produces a coarser microstructure and leads to the reduction of fracture toughness in the weld.

Key words: Invar 36 alloy; friction stir welding; fracture toughness; small punch test

Optimization of parameters and joint microstructure of electrode beam welding of 2A14 Al alloy WANG Yarong,